

# Evoked Potentials Recorded From the Spinal Cord During Neurostimulation for Pain: A Computational Modeling Study

Carlos J. Anaya, BS\*<sup>†</sup>; Hans J. Zander, MSE\*<sup>†</sup>; Robert D. Graham, MSE\*<sup>†</sup>; Vishwanath Sankarasubramanian, PhD\*<sup>†</sup>; Scott F. Lempka, PhD\*<sup>†‡</sup>

**Objectives:** Spinal cord stimulation (SCS) for pain is typically implemented in an open-loop manner using parameters that remain largely unchanged. To improve the overall efficacy and consistency of SCS, one closed-loop approach proposes to use evoked compound action potentials (ECAPs) recorded from the SCS lead(s) as a feedback control signal to guide parameter selection. The goal of this study was to use a computational modeling approach to investigate the source of these ECAP recordings and technical and physiological factors that affect their composition.

**Methods:** We developed a computational model that coupled a finite element model of lower thoracic SCS with multicompartiment models of sensory axons within the spinal cord. We used a reciprocity-based approach to calculate SCS-induced ECAPs recorded from the SCS lead.

**Results:** Our model ECAPs contained a triphasic, P1, N1, P2 morphology. The model P2-N1 amplitudes and conduction velocities agreed with previous experimental data from human subjects. Model results suggested that the ECAPs are dominated by the activation of axons with diameters 8.7–10.0  $\mu\text{m}$  located in the dorsal aspect of the spinal cord. We also observed changes in the ECAP amplitude and shape due to the electrode location relative to the vertebrae and spinal cord.

**Conclusion:** Our modeling results suggest that clinically effective SCS relies on the activation of numerous axons within a narrow fiber diameter range and that several factors affect the composition of the ECAP recordings. These results can improve how we interpret and implement these recordings in a potential closed-loop approach to SCS.

**Keywords:** Chronic pain, computer simulation, evoked potentials, spinal cord, spinal cord stimulation

**Conflict of Interest:** Dr. Lempka holds stock options with Presidio Medical, Inc., and serves on the scientific advisory board. All other authors declare no conflicts of interest.

## INTRODUCTION

Spinal cord stimulation (SCS) is a common neuromodulation therapy for chronic pain conditions (e.g., failed back surgery syndrome) that are often refractory to conventional treatments. The goal of conventional SCS is to deliver electrical stimulation to the large-diameter afferent axons located within the dorsal columns (DCs) of the spinal cord in an attempt to create analgesia via “gating” mechanisms of pain modulation (1,2). However, even after decades of clinical use and dramatic technological improvements, SCS has shown only limited success rates (approximately 58% of patients receive  $\geq 50\%$  reduction in pain) (3).

To potentially improve clinical outcomes, a novel closed-loop SCS paradigm has been proposed that utilizes evoked compound action potentials (ECAPs) in the spinal cord as a feedback control signal for stimulation (4,5). This approach uses inactive electrodes in the implanted SCS arrays to record ECAPs generated during SCS. These ECAPs reflect the summation of individual action potentials generated by an SCS pulse and provide a quantitative measure of neural recruitment in the spinal cord. The ECAP amplitude serves as a control signal to continuously define stimulation parameters that provide pain relief while minimizing discomfort. While the therapeutic potential of this approach was demonstrated in a recent open-label uncontrolled clinical study (5), the physiological factors influencing

these recordings has not been thoroughly investigated. This knowledge gap may limit our ability to use this type of closed-loop approach to optimize SCS-induced analgesia.

Experimental recordings of spinal cord ECAPs in humans reported a triphasic morphology—an initial positive wave (P1), followed by a sharp negative peak (N1), and ending with a second positive wave (P2)—and conduction velocities that varied from 37 m/s and

Address correspondence to: Scott F. Lempka, PhD, Department of Biomedical Engineering, University of Michigan, 2800 Plymouth Road, NCRC 014-184, Ann Arbor, MI 48109-2800, USA. Email: lempka@umich.edu

\* Department of Biomedical Engineering, University of Michigan, Ann Arbor, MI, USA;

<sup>†</sup> BioInterfaces Institute, University of Michigan, Ann Arbor, MI, USA; and

<sup>‡</sup> Department of Anesthesiology, University of Michigan, Ann Arbor, MI, USA

For more information on author guidelines, an explanation of our peer review process, and conflict of interest informed consent policies, please go to <http://www.wiley.com/WileyCDA/Section/id-301854.html>

Source(s) of financial support: This research was supported in part by the National Institutes of Health (NIH R01 NS089530), and the University of Michigan Rackham Merit Fellowship Program. This work used the Extreme Science and Engineering Discovery Environment (XSEDE), which is supported by the National Science Foundation grant number ACI-1548562, resource Comet at the San Diego Supercomputer Center.

up to 82 m/s depending on the study (6–8). A study by Parker et al. demonstrated that it was possible to record these ECAPs during clinical SCS by using the inactive electrodes on the implanted SCS trial lead (9). The authors reported that the ECAP amplitude was correlated with the degree of SCS-induced paresthesia coverage over the painful area. The ECAP recordings demonstrated conduction velocities in the range of 49–65 m/s, suggesting that SCS activated axons with diameters between 8.1–10.8  $\mu\text{m}$  (9).

Several factors may affect neural recruitment during SCS and the corresponding spinal ECAP. For example, SCS-induced ECAPs recorded in a sheep model showed that the ECAP amplitude was attenuated when stimulation and recording was performed on electrodes located beneath the vertebral lamina (10). The spinal cord also moves due to changes in body position (e.g., standing, sitting, and prone) as well as respiration and heartbeat (11). This movement alters the distance between the spinal cord and the stimulating electrodes and can lead to overstimulation or under-stimulation for a given set of stimulation parameters. A closed-loop SCS system using ECAPs as a control signal may improve outcomes by accounting for these potential changes in the distance between the spinal cord and the stimulating electrodes. The feasibility of this type of closed-loop approach was demonstrated in a preliminary clinical study in which  $\geq 80\%$  of patients experienced a  $\geq 50\%$  reduction in their pain (5). However, there is still a lack of understanding behind the origin of these ECAPs and the various technical and physiological factors that affect the composition of these recordings. Addressing this knowledge gap could help optimize the clinical efficacy of this type of closed-loop approach in SCS.

Computational modeling has been used to investigate the physiological and technical factors that affect the direct neural response to SCS (12–18). The aim of this study was to use computational modeling to characterize the composition of ECAP recordings during SCS. We developed a computational model that coupled a finite element model of lower thoracic SCS with multicompartment models of sensory axons to calculate ECAP signals recorded from the spinal cord during stimulation. We hypothesized that the specific fiber-diameter distribution within the DC of the spinal cord would be responsible for the characteristics of SCS-induced ECAPs. Additionally, we assessed the potential effects of electrode location and dorsal CSF thickness on the amplitude and morphology of SCS-induced ECAP recordings. We hypothesized that ECAP amplitude and shape would be affected by electrode position relative to the vertebrae, electrode position relative to the spinal midline, and dorsal CSF-layer thickness.

## MATERIALS AND METHODS

We used a computational model of SCS to calculate ECAPs recorded via inactive electrodes in the implanted lead. The computational model consisted of two main components: 1) a finite element model (FEM) of an SCS lead implanted in the dorsal epidural space of the spinal cord; and 2) multicompartment cable models of spinal cord DC axons. We calculated ECAPs during SCS using the following procedure: 1) we used the FEM to calculate the extracellular voltages generated in the spinal cord and surrounding tissues during SCS; 2) we populated the spinal cord white matter with multicompartment cable models of sensory axons; 3) we assessed the direct axonal response to SCS by applying the extracellular voltages to the sensory axon models to

obtain transmembrane currents in response to stimulation; and 4) we calculated the SCS-induced ECAP by using a reciprocal FEM solution to determine the voltage generated at each recording electrode.

### Finite Element Model of SCS

First, we developed a three-dimensional finite element model (FEM) of lower thoracic SCS to calculate the extracellular voltages generated during stimulation (Fig. 1a). The model consisted of the gray and white matter of the spinal cord and dorsal rootlets, surrounded by CSF, dura matter, as well as epidural fat filling the extradural space and a three-dimensional anatomical representation of the vertebral column including intervertebral discs (19). The dimensions of the spinal cord and the gray and white matter boundaries were defined by human cadaver samples of the lower thoracic spinal cord (20). We placed five dorsal rootlets with diameters of 0.25 mm at each spinal level (21). Unless specified otherwise, we set the dorsal CSF-layer thickness to 3.2 mm (22) and the dura thickness to 300  $\mu\text{m}$  with the dorsal surface flattened for computational simplicity (13,17). We stacked seven identical and anatomically-accurate T9 vertebrae in the rostrocaudal direction to make the vertebral column with intervertebral discs based on a previously-published model (19). We included an explicit representation of an eight-electrode percutaneous lead implanted in the epidural tissue. The SCS lead dimensions mimicked the electrodes used in previously-reported experimental recordings (9), with 1.3 mm lead diameter, 30 cm lead length, 3 mm contact length, and 4 mm edge-to-edge contact spacing. To mimic scar tissue formation around the implanted SCS lead, we included a 300  $\mu\text{m}$ -thick encapsulation layer domain surrounding the lead (23). We placed the spinal column inside a general thorax domain mimicking the anatomy observed in healthy humans (24,25). We used the 3-matic module within the mimics innovation suite (Materialize, Belgium) to define and mesh the model geometry. We specified higher mesh densities at the electrode array and encapsulation layer as well as within a 64-mm long region of interest surrounding the electrodes.

We imported the FEM into the finite element analysis software, COMSOL Multiphysics 5.3a (Comsol, Inc., MA, USA). We modeled each tissue using purely resistive properties, and we assigned electrical conductivity values using values available in the literature (16,17,23) (Table 1). We set the encapsulation layer conductivity to 0.11 S/m (23) so that the average model monopolar electrode impedances (359  $\Omega$ ) matched average clinical values (13). We used the most caudal electrode (C7) as the stimulating electrode. To simulate current-controlled monopolar stimulation, we applied a unit current source at the stimulating electrode (i.e., 1A) and set the outer-most boundaries of the general thorax domain to ground (i.e., 0 V). We modeled the SCS lead shaft as a perfect insulator and we modeled inactive electrodes as equipotential across each of their respective surfaces (Robin boundary condition). We solved the Laplace equation and calculated the resulting voltages at each point in the FEM.

### Multicompartment Cable Model of Sensory Axons

Second, we developed computer models of sensory axons within the DCs of the spinal cord. Our multicompartment cable models of DC sensory axons were based on a previously-published model of a mammalian sensory axon for specific fiber diameters that was parametrized to accurately reproduce conduction velocities, action

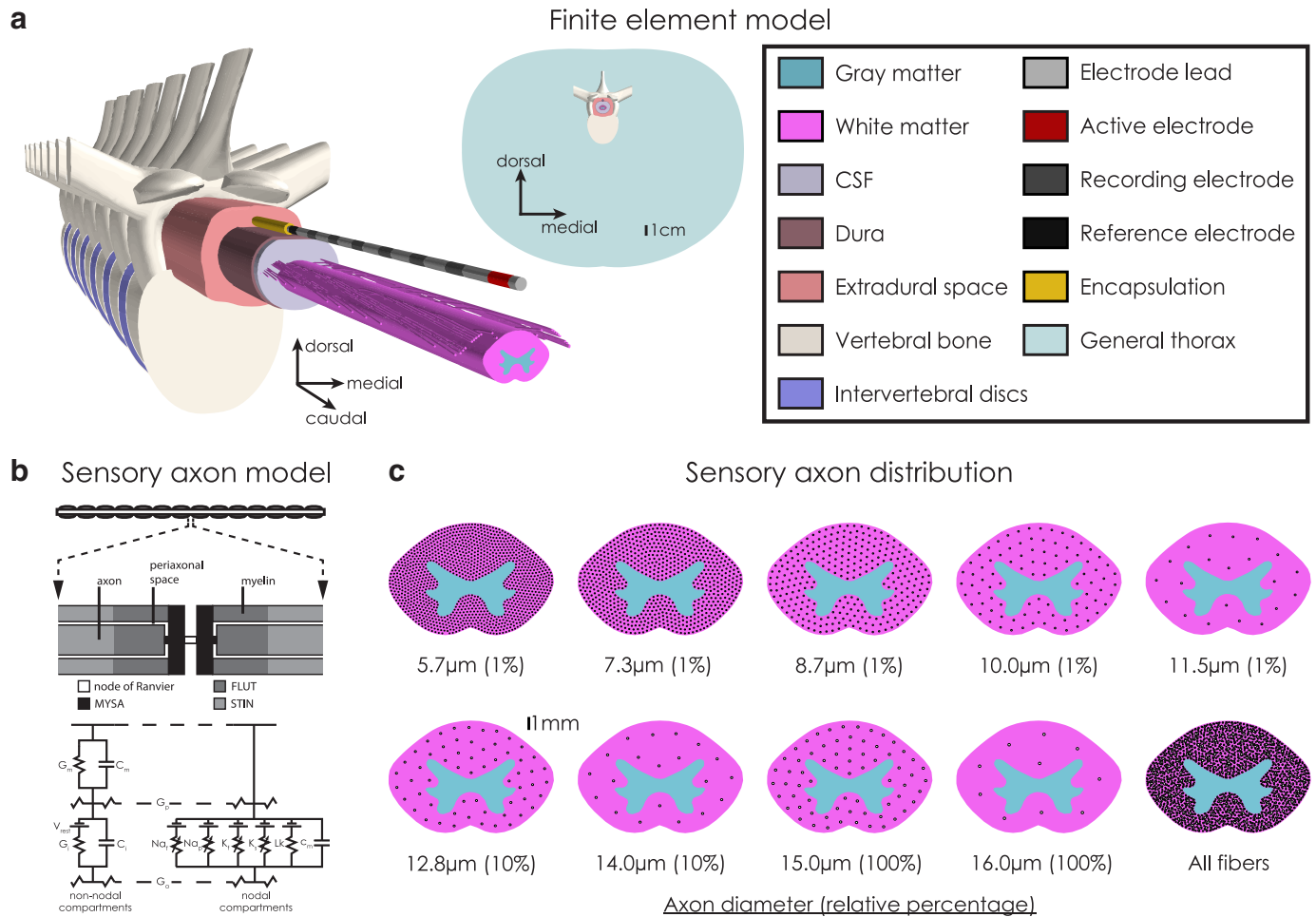


**Figure 1.** Computational model of spinal cord stimulation (SCS). a. Finite element model of the lower thoracic spinal cord with surrounding anatomy and an eight-electrode SCS lead implanted in the extradural space. Isometric and axial views of the model are shown on the left and middle, respectively. b. Sensory axon model of DC fibers. Figure was adapted from (29). c. Distribution of sensory axons in the spinal cord for each discrete fiber diameter. We determined the density of each fiber size using previously-published histological data from the human spinal cord (30). For computational simplicity, we populated our model with only a relative percentage of the total physiological densities and scaled the results accordingly. [Color figure can be viewed at wileyonlinelibrary.com]

potential shape, and strength-duration relationships for sensory axons (26–29) (Fig. 1b). For this study, we considered axon diameters of 5.7–16.0  $\mu$ m with densities based on histological data of the

Tissue	Electrical conductivity (S/m)
White matter (longitudinal)	0.600
White matter (transverse)	0.083
Gray matter	0.230
Cerebrospinal fluid	1.700
Dura matter	0.600
Extradural space	0.250
Vertebral bone	0.020
Intervertebral disc	0.650
General thorax	0.250
Electrode encapsulation	0.110

human spinal cord (30). We first divided the histological data describing axon number as a function of diameter into the discrete axon diameters that were available for the given axon model (i.e., 5.7, 7.3, 8.7, 10.0, 11.5, 12.8, 14.0, 15.0, and 16.0  $\mu$ m) (26,29). Second, we normalized this data to determine the percentage of axons within each specified diameter range. Third, to calculate the density of axons for a given diameter, we multiplied the percentage of axons by the total density of axons per area (i.e., 22.92 axons/1000  $\mu$ m<sup>2</sup>) (30). Finally, to determine the total number of axons for a given diameter, we then multiplied the individual axon density by the cross-sectional area of our model white matter (i.e., 23.62 mm<sup>2</sup>). The spinal cord DC is densely populated by small diameter axons and contains fewer more dispersed large diameter axons (30). To ease computational demand while properly modeling the density of each individual fiber diameter, we selectively used a fraction of the true anatomical densities for each fiber diameter: 1% for diameters  $\leq$ 11.5  $\mu$ m, 10% for diameters of 12.7 and 14.0  $\mu$ m, and 100% for diameters  $\geq$ 15.0  $\mu$ m (Fig. 1c). When calculating the model ECAP, we scaled the relative signal contribution from each fiber size by the appropriate scale factor to achieve 100% of the true anatomical density. We distributed each fiber diameter

group evenly within the white matter boundaries using Lloyd's algorithm (31) (Fig. 1c).

### Assessment of the Direct Axonal Response to SCS

We assessed the direct axonal response to SCS by applying the extracellular voltages calculated in our FEM to each compartment of our sensory axon cable models. We performed simulations for stimulation amplitudes between 1–10 mA, in 1 mA steps, using a cathodic, monophasic stimulus waveform with a frequency of 50 Hz and a pulse width of 210  $\mu$ s. We performed all axon simulations with the software package, NEURON, within the Python programming environment using a supercomputer cluster (32,33). We calculated model solutions using backward Euler implicit integration with a time step of 0.002 ms.

### Calculation of ECAP Recordings

To simulate ECAP recordings, we used the theorem of reciprocity to calculate the time-dependent voltages generated at each electrode by the axonal response to SCS (34–38). We applied a unit current source (i.e., 1A) at the individual recording electrode, grounded the outer-most boundaries of the general thorax (i.e., 0 V), applied Robin boundary conditions at the other electrodes, and solved the Laplace equation to obtain the resulting model tissue voltages. We interpolated the resulting voltages onto each axonal compartment, interpreting this voltage as the voltage impressed onto the recording electrode by a unit (i.e., 1A) current source placed at the spatial location of each compartment. We calculated the ECAP by superimposing the voltages generated at the recording electrode from the scaled transmembrane currents of each independent compartment. We repeated this process for each recording electrode and obtained bipolar differential recordings using the most rostral electrode (i.e., C0) as a reference signal, subtracting it from each recording electrode. To mimic the processing done experimentally, we low-pass filtered each signal at 7.5 kHz using a two-pole low-pass Butterworth filter (9).

### Evaluation of Model ECAP Recordings

To characterize our model ECAP recordings, we defined a model sensory threshold (ST) and discomfort threshold (DT). The ST was defined as the stimulus amplitude that resulted in activation of  $\geq 10\%$  of the DC fibers in the spinal cord, and the DT was defined as  $1.4 * ST$  (13,15,16,39). We defined the ECAP amplitude as the difference between the P2 and N1 peak amplitudes, ECAP spread as the full width of the signal at half the N1 peak maximum value (FWHM), and ECAP conduction velocity as the time difference between the N1 peaks recorded at adjacent contacts divided by the center-to-center distance between adjacent electrodes (i.e., 7 mm) (6–9,18).

We explored the effects of electrode position relative to the vertebrae, lead lateral shift, and dorsal CSF-layer thickness on SCS-induced ECAP recording waveform shape and amplitude. In our base model, we placed the lead so that the middle electrode (C3) was centered between adjacent vertebral laminae (Fig. 2a). We then shifted the lead along the rostrocaudal axis by 11.8 mm to center electrode C3 beneath the vertebral lamina to account for any effects of electrode location relative to the vertebrae. Additionally, we characterized the effects of lead lateral displacement by shifting the lead 2.0 mm lateral from the spinal cord midline. Lastly, the amount of CSF between the dura and the spinal cord varies significantly as a function of spinal level, varies

between patients, and changes with movement, heartbeat, and respiration (22). To account for these changes, we shifted the spinal cord along the dorsoventral axis to vary the dorsal CSF-layer thickness between 2.0, 3.2, and 4.4 mm to observe the effects of CSF-layer thickness on the recordings. We calculated each model's ST and DT and compared each model's C3–C0 bipolar ECAP recording at DT. To avoid potential confounds due to differences in stimulation-induced axonal response between models, we also calculated each model ECAP using the same neural response generated with the base model conditions (i.e., C3 electrode centered between adjacent vertebral laminae, the lead placed at the spinal cord midline, and a dorsal CSF-layer thickness of 3.2 mm).

## RESULTS

### Model-Based ECAP Recordings

We calculated model ECAP recordings induced by SCS, with a lead placed in the dorsal epidural space at lower thoracic spinal levels. In our model, we estimated a ST of 6 mA (i.e.,  $\geq 10\%$  of DC fiber activation) (15,16) and a corresponding DT of 8 mA (i.e.,  $1.4 * ST$ ) (13,39) for monopolar stimulation applied at electrode, C7 (frequency = 50 Hz, pulse width = 210  $\mu$ s) (Fig. 2a). Therefore, we assumed a model-based therapeutic window of 6–8 mA. The model ECAP exhibited a triphasic shape, starting with a positive P1 peak, followed by a sharp negative N1 peak, and ending with a second positive P2 peak for both monopolar and bipolar ECAP recordings (Fig. 2b). The signals recorded on electrodes far from the stimulating electrode are smaller and more spread out as the signals in each fiber-diameter group propagate at different velocities. A stimulus artifact precedes the model ECAP recording due to the response to the electrical stimulus of the membrane capacitance at the nodes of Ranvier (37). We compared our model ECAP at the DT with a clinical ECAP recording performed on an electrode 28-mm away from the stimulating electrode (9) (Fig. 2c). Both the clinical and model recordings contain the N1 and P2 peaks of the triphasic spinal ECAP morphology, with a similar N1 peak latency, and a P2–N1 amplitude of 200 and 216  $\mu$ V for the clinical and model ECAPs, respectively. The clinical ECAP recording contains a large stimulus artifact from the recording electrodes being in close proximity to the stimulating electrodes (9). This large stimulus artifact affects the detection of the P1 peak observed in the model ECAP recording for electrodes near the stimulating electrode.

### ECAP Properties—Stimulation Amplitude

We calculated ECAPs for stimulus amplitudes over the range of 1–10 mA (Fig. 3a). The P2–N1 amplitude increased linearly over this range of stimulus amplitudes (Fig. 3b). As the stimulus amplitude was increased, the ECAP P2–N1 amplitude increased, but the latency of the N1 peak stayed relatively constant. At lower stimulus amplitudes (i.e., 3 mA), the ECAP conduction velocity was higher ( $\sim 78$  m/s) (Fig. 3c). At higher stimulus amplitudes (i.e.,  $\geq 4$  mA), smaller diameter fibers were activated and the ECAP conduction velocity decreased to an average value of 53.5 m/s. The FWHM is the width of the N1 waveform at half its peak value and can provide information about the range of fiber diameters captured by the ECAP N1 wave. The FWHM increased linearly at lower stimulation amplitudes but plateaued before reaching the therapeutic window (Fig. 3d), and it showed that the relative

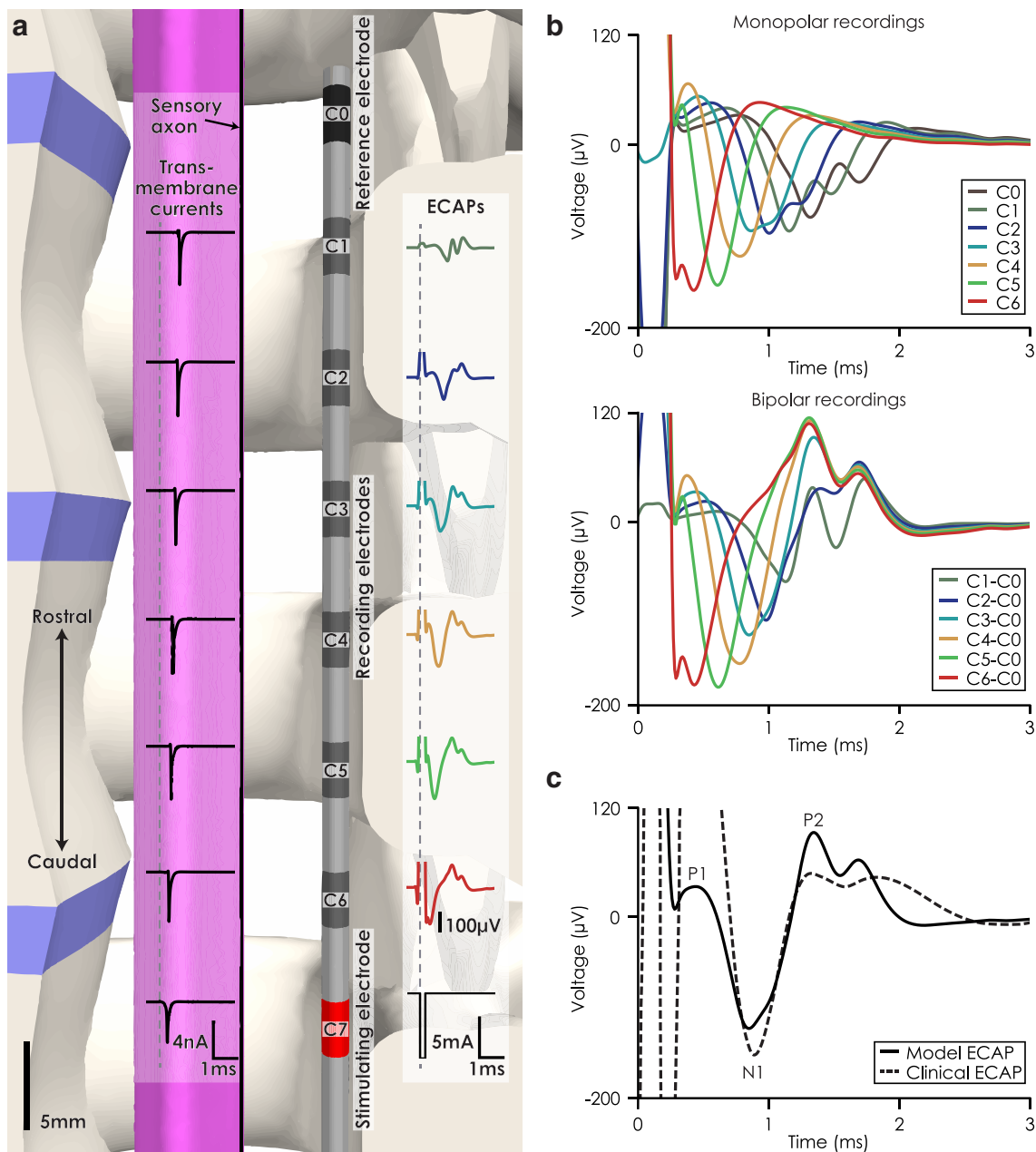


**Figure 2.** Model-based recordings of evoked compound action potentials (ECAP) induced by SCS. **a** Sagittal cross section view of the spinal cord, SCS lead, and surrounding vertebral bone and discs. In the traces overlapping the spinal cord, we show an example of the transmembrane currents generated in a single axon in response to a monophasic stimulus pulse. In the traces on the right, we show the stimulus pulse as well as bipolar recordings of the summed response of all axons in our model. The dashed lines represent the time of stimulus onset. **b** ECAP recordings at each contact for monopolar and bipolar (referenced to C0) configurations. **c** A bipolar (C3-C0) model ECAP recording compared to a previously-reported clinical ECAP recording (see Fig. 5b in (9)). The model and clinical ECAP recordings were obtained at stimulation amplitudes near the model-based discomfort threshold and the patient comfort threshold, respectively. [Color figure can be viewed at [wileyonlinelibrary.com](http://wileyonlinelibrary.com)]

proportion of fiber diameters recruited and captured in the N1 peak, stayed relatively constant with any further increase in stimulation amplitude.

#### ECAP Composition—Axon Size

We measured the percentage of each fiber-diameter group recruited at each stimulation amplitude (Fig. 4a). We observed fiber activation starting at a minimum stimulus amplitude of 2 mA, which only recruited fibers >12.0 µm. Within the model-based

therapeutic window, the largest percentages of activated fibers had diameters of 7.3, 8.7, and 10.0 µm. To determine the corresponding relative contribution of each fiber diameter to the measured ECAP at each stimulation amplitude, we calculated the individual signal for each fiber diameter group alongside the overall model ECAP (Fig. 4b). We quantified the contribution of each fiber diameter group to the total ECAP amplitude by removing each individual group from the overall ECAP (Fig. 4c). For 7.3 µm fibers, the percent difference in ECAP amplitude after removing these fibers from the ECAP was -11.0% and -13.1% measured at

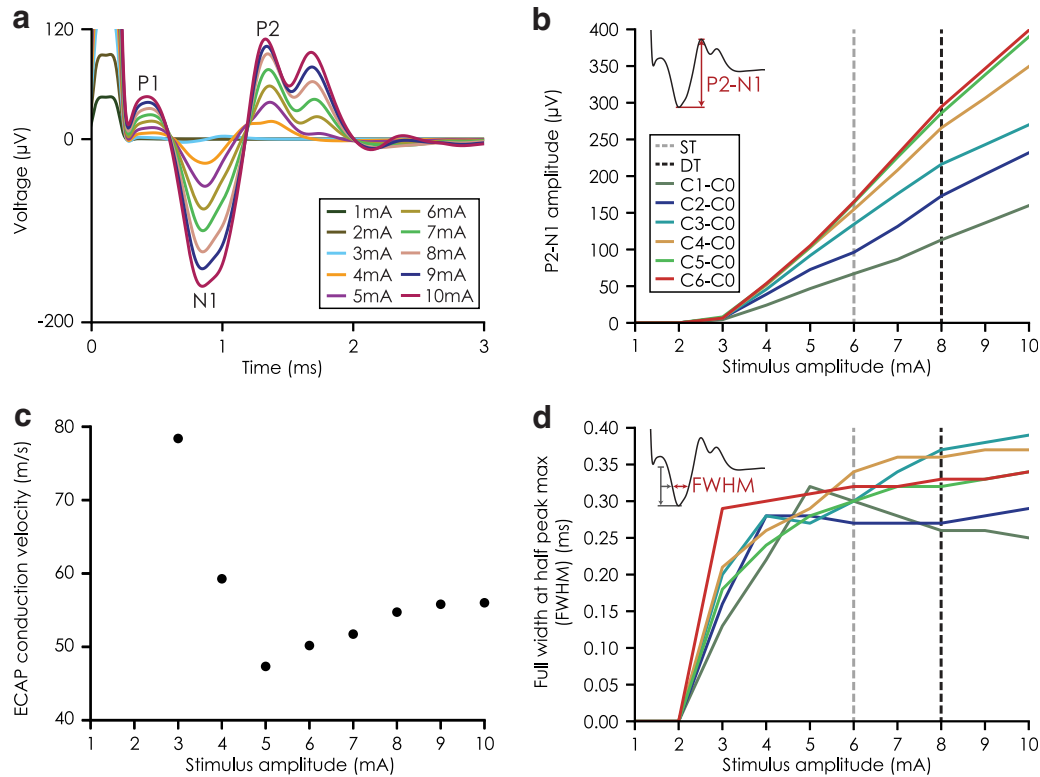


**Figure 3.** SCS-induced ECAP recordings as a function of stimulus amplitude. a. Bipolar ECAP recordings from electrodes, C3-C0, as function of stimulus amplitude. b. P2-N1 amplitude as a function of stimulus amplitude. c. ECAP conduction velocities as a function of stimulus amplitude, measured using the N1 latency difference between neighboring electrodes. d. ECAP full width at half max (FWHM) as a function of stimulus amplitude. In b and d, the model-based therapeutic range is highlighted by dashed lines at the sensory threshold (ST) and discomfort threshold (DT). [Color figure can be viewed at [wileyonlinelibrary.com](http://wileyonlinelibrary.com)]

ST and DT, respectively. For 8.7  $\mu\text{m}$  fibers, the percent difference was  $-35.0\%$  and  $-39.4\%$  measured at ST and DT, respectively. For 10.0  $\mu\text{m}$  fibers, the percent difference was  $-30.6\%$  and  $-27.4\%$  measured at ST and DT, respectively. For 11.5  $\mu\text{m}$  fibers, the percent difference was  $-8.3\%$  and  $-7.2\%$  for ST and DT, respectively. For all fibers with diameter  $\geq 12.8 \mu\text{m}$ , the percent difference was  $-4.5\%$  and  $-3.2\%$  for ST and DT, respectively. Only a few fibers with a diameter of 5.7  $\mu\text{m}$  were recruited within the therapeutic window (i.e.,  $<2.5\%$ ) and removing these fibers only produced a percent difference of 0.0% and  $-0.4\%$  for ST and DT, respectively. These results demonstrate that the 8.7 and 10.0  $\mu\text{m}$  fibers had the greatest contributions to the overall ECAP amplitude (i.e., P2-N1).

**ECAP Size and Shape—Anatomical Considerations**

We considered three conditions that could potentially affect stimulation thresholds and the corresponding ECAP recording during clinical SCS: 1) electrode position relative to the vertebrae; 2) lead lateral shift; and 3) thickness of the dorsal CSF-layer (Fig. 5). To test the effects of electrode location relative to the vertebral column on ECAP recordings, we shifted the position of the recording electrode, C3, so that it was centered beneath the vertebral lamina (Fig. 5a). When the electrode is centered beneath the vertebral lamina, there was a minimal increase in the number of fibers recruited by stimulation. This shift in electrode position increased the P2-N1 amplitude but had virtually no effect on the waveform morphology (Fig. 5a). Although a lateral shift in lead location activated fibers at different spatial locations within the DC, it produced a minimal difference in the overall number of

recruited fibers and minimal differences in the corresponding ECAP shape and amplitude (Fig. 5b). Lastly, increasing the thickness of the dorsal CSF-layer increased the stimulus amplitude required to reach ST (ST = 4, 6, and 9 mA for 2.0, 3.2, and 4.4 mm thickness, respectively). The P2-N1 amplitude decreased and the increase in distance between the electrode and the spinal cord exerted a low-pass filtering effect on the waveform shape, apparent in the P2 peak morphology (Fig. 5c). We also compared model ECAP recordings calculated using the same underlying neural activity (i.e., neural activation produced in the base model conditions with C3 centered between lamina, the lead placed at the spinal cord midline, and a dorsal CSF thickness of 3.2 mm) for each set of model conditions with different lead or spinal cord positions. Even with the same underlying neural activity, we observed similar effects on ECAP size and shape for each condition (data not shown). Therefore, the trends observed under the different model conditions were largely attributed to changes in the lead and/or spinal cord position and not due to corresponding differences in neural recruitment.

**DISCUSSION**

We developed a computational model of SCS to characterize ECAP signals recorded from the spinal cord. We coupled a FEM and multicompartment models of spinal cord axons to calculate ECAPs recorded from inactive electrodes. We calculated ECAPs over a range of stimulus amplitudes and defined a model-based therapeutic window. We then examined the effects of the lead

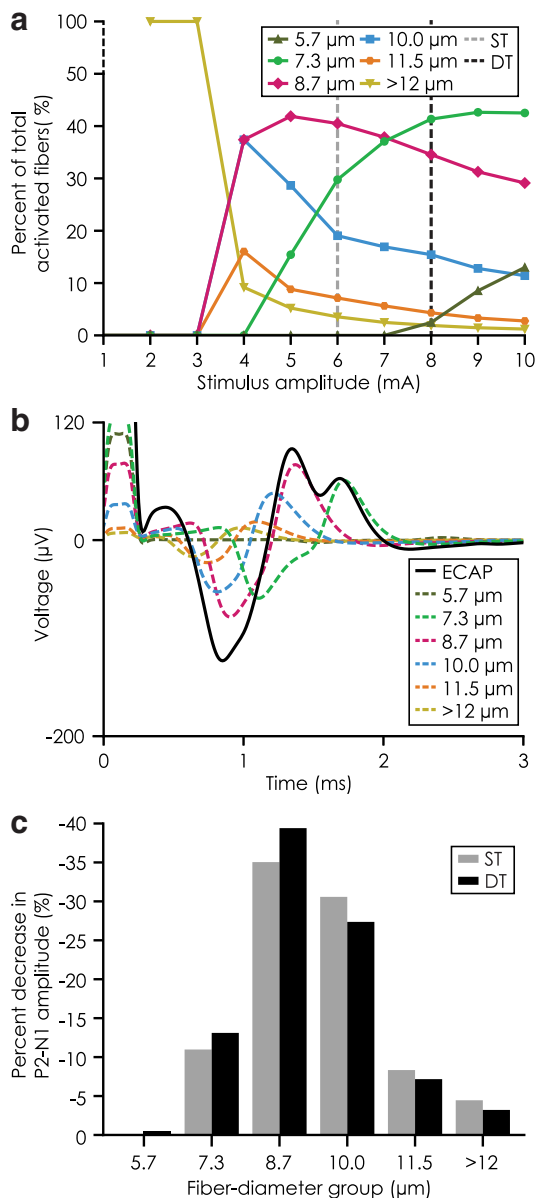


**Figure 4.** Contribution of fiber size to the overall ECAP waveform. a. Relative contributions of each fiber size to the total number of fibers activated at a given stimulus amplitude. Dashed lines indicate an axis break to 100%. The model-based therapeutic range is highlighted by dashed lines at the sensory threshold (ST) and discomfort threshold (DT). b. Overall ECAP waveform along with the individual ECAPs generated by each fiber-diameter group at a stimulus amplitude of 8 mA. c. Percent decrease in P2-N1 amplitude when an individual fiber-diameter group was removed from the ECAP recording at the model-based ST and DT. [Color figure can be viewed at [wileyonlinelibrary.com](http://wileyonlinelibrary.com)]

location relative to the spine and spinal cord on the ECAP size and shape.

#### SCS-Induced ECAPs and Fiber Recruitment During Clinical SCS

At the model-based DT, our model ECAPs resembled clinical recordings taken at the patient's comfort limit, that is, triphasic morphology, similar N1 peak latency, and a similar P2-N1 amplitude (Fig. 2c) (9). Within the therapeutic window, we observed a linear relationship between the measured P2-N1 amplitude and stimulus amplitude (Fig. 3b). This trend was also observed

experimentally in humans and a sheep model of SCS-induced ECAPs (9,10). For stimulation amplitudes within the therapeutic window, our model ECAP conduction velocities remained relatively constant with a range of 47–59 m/s. This trend was similar to clinical observations in which the conduction velocities remained relatively constant irrespective of the stimulation amplitude with a range of 49–65 m/s (9).

To examine the range of fiber sizes recruited by clinical SCS, we designed our model to include physiological fiber sizes and densities within the spinal cord (30). We then considered the relative contribution of different fiber sizes to the SCS-induced ECAP by examining how removing individual fiber-diameter groups affected the overall ECAP. Removing fiber diameters of 8.7 and 10.0 μm from the ECAP produced the largest percent decrease in the measured ECAP amplitude (i.e., –35 and –31% at ST, respectively) (Fig. 4c). This result can also help us to understand the type of fibers that are recruited in clinically effective SCS. In a previous clinical study, Parker et al. demonstrated a correlation between the ECAP amplitude and the degree of paresthesia overlap with the painful area (9). Because conventional SCS may require pain-paresthesia overlap (4), DC fibers with diameters  $\geq 8.7$  μm are most likely activated during clinically effective stimulation.

#### Anatomical Considerations in SCS-Induced ECAP Recordings

In this study, we used our model to investigate a number of anatomical factors relevant to SCS that might affect the size and/or shape of the ECAP recordings. Our FEM included a realistic anatomical representation of the spine, which allowed us to investigate how electrode location relative to the vertebrae affects ECAP recordings. Parker et al. observed differences in the P2-N1 amplitude that were potentially related to electrode location relative to structures of the sheep vertebral column (10). Similarly, we observed an increase in the ECAP amplitude for electrodes located beneath the vertebral lamina relative to electrodes located between two adjacent laminae (Fig. 5a). These results were similar when the two model conditions were compared using the same underlying neural activity (data not shown). Therefore, our results suggest that electrodes may have different recording amplitudes based on their relative position along the vertebral column.

Lead migration is common in SCS, especially with percutaneous leads (40), and could result in changes in the ECAP recordings. Our results showed that a 2-mm lateral shift in lead position relative to the spinal cord midline produced no appreciable change in the ECAP amplitude and shape (Fig. 5b). Our model results are similar to spinal potential recordings performed in human volunteers, where the position of an intrathecal recording microelectrode along the mediolateral axis did not affect the magnitude and shape of the recorded signal (7). These results suggest that the mediolateral location of the recording electrodes will minimally affect the size and shape of the ECAP recording.

The clinical efficacy of a given set of SCS parameters can vary with movement of the spinal cord that occurs due to postural changes, heartbeat, and respiration (11). It is estimated that the spinal cord can move ~2–3 mm in the anterior–posterior direction at the lower thoracic spinal levels and can increase or decrease the distance between the spinal cord and the SCS electrodes. Therefore, this movement can lead to overstimulation or understimulation and a corresponding change in the ECAP amplitude (9). To investigate the effects of spinal cord movement on the corresponding ECAP, we varied the thickness of the

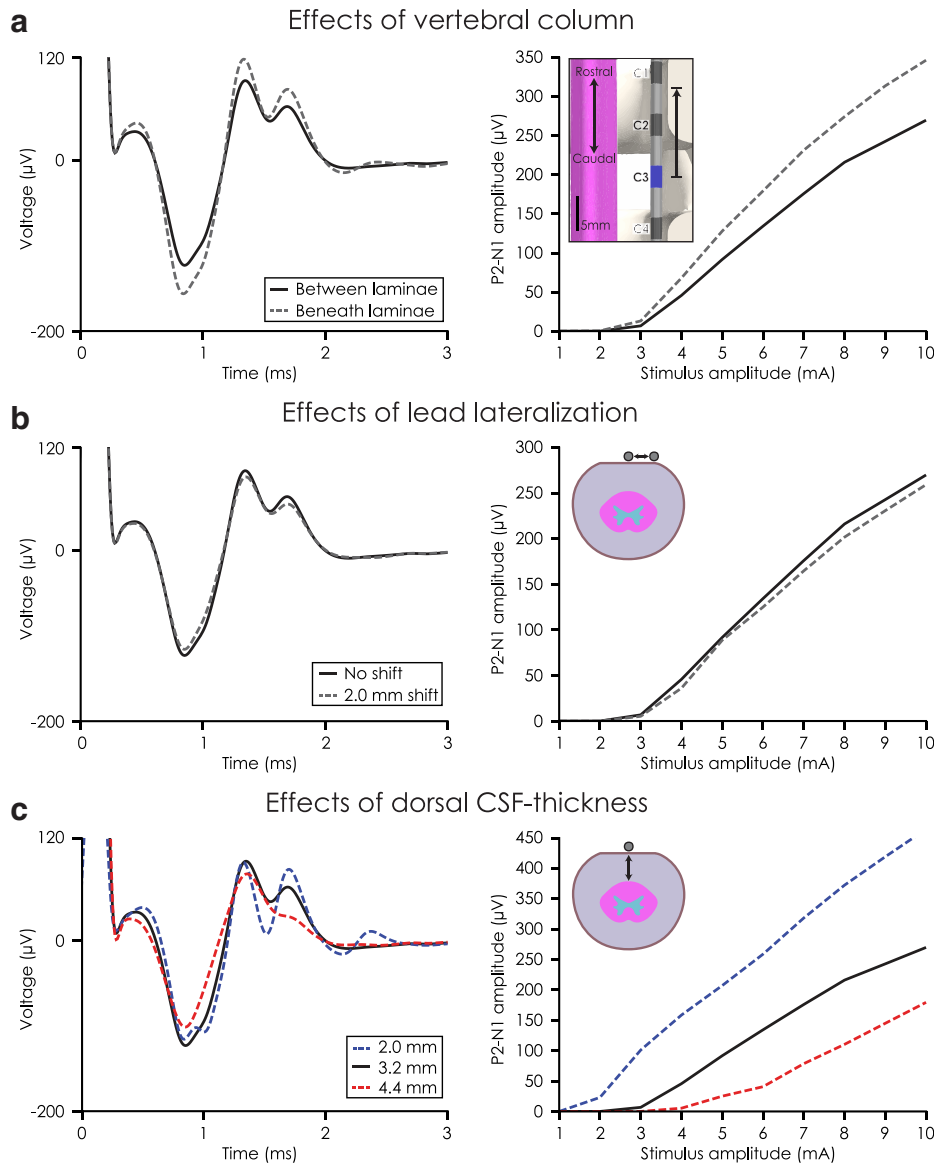


**Figure 5.** Effects of electrode and spinal cord position on ECAP recordings. a. To examine the effect of electrode position relative to the spine, we considered the ECAP with the recording electrode (C3) centered between two vertebral laminae and with the recording electrode centered directly beneath the vertebral lamina (see inset on right). b. To examine the effect of a lateral lead placement, we obtained model-based ECAP recordings with the lead centered at the spinal cord midline and the lead shifted 2 mm lateral (see inset on right). c. To examine the effect of spinal cord position, we moved the spinal cord in the anterior–posterior direction and calculated model-based ECAPs for dorsal CSF thicknesses of 2.0, 3.2, and 4.4 mm (see inset on right). Plots in the left column show the ECAP recordings at each model determined discomfort threshold, while the plots in the right column show the corresponding ECAP amplitude as a function of stimulus amplitude. [Color figure can be viewed at [wileyonlinelibrary.com](http://wileyonlinelibrary.com)]

dorsal CSF-layer within our model (Fig. 5c). As the dorsal CSF-layer thickness was increased, the model-based ST increased and the ECAP amplitude decreased. Additionally, the increase in distance between the spinal cord and recording electrode affected the shape of the P2 component, smoothing the morphology of the signal. To isolate the effects of electrode-to-cord distance, we also investigated these changes while using the same underlying neural activity in our simulations. With an increase in dorsal CSF-layer thickness and the same underlying neural activity, we observed a similar decrease in ECAP amplitude and a low-pass filtering effect that smoothed the morphology of the waveform (data not shown). Changes in the electrode-to-cord distance can lead to significant changes in the ECAP amplitude and these trends occur even for the same underlying neural activity. In closed-loop SCS, stimulation

amplitude is controlled to maintain ECAP amplitude within a specific range in an attempt to maintain more consistent levels of activation within the spinal cord (5). To optimize this approach, closed-loop SCS algorithms should consider possible changes in ECAP amplitude that may occur solely due to differences in the electrode-to-cord distance.

**Study Limitations and Future Work**

In this study, we utilized multicompartment models of sensory axons in the white matter of the spinal cord as the electrical source in our ECAP recordings. These sensory axon models have previously been shown to accurately model the behavior of sensory axons for discrete fiber diameters within the range of

diameters used in this study (26,27,29). Since only discrete fiber sizes were used, differences in conduction velocities in the propagating action potentials of different fiber-diameter groups led to differences in the P2 peak morphology of our model ECAPs when compared to the clinical ECAP recordings (Fig. 2c). Additional neuron models, such as dorsal horn neurons, were excluded from our analysis. Even though only a small percent of current (<10%) is believed to enter the spinal cord during SCS (12), it may be possible to excite dorsal horn neurons at high stimulus amplitudes and somatic action potentials from these neurons have been hypothesized to produce a late potential in the ECAP following the initial triphasic wave (7). However, in humans, these late potentials were only observed at stimulation amplitudes well above a patient's comfort limit (9). Future work should investigate the extent to which activity in the dorsal horn affects recordings beyond the therapeutic window, as it might provide insights into the nature of the discomfort caused by overstimulation.

Currently, no clear relationship has been established between clinical measurements of ST or DT and the corresponding degrees of DC neural activation. In this study, we defined a model-based ST as  $\geq 10\%$  activation of DC fibers and DT as  $1.4 * ST$  to compare the trends observed in our model ECAPs with previously-published clinical ECAP recordings (9). These assumptions are a potential limitation of our study; however, other recent SCS modeling studies have used a similar percentage of DC activation to estimate ST and motor thresholds that produced results that matched well with clinical and preclinical measurements (15,16,41). Furthermore, the DT has previously been defined as  $1.4 * ST$  based on clinical observations and has also been used in previous modeling studies as an approximation for DT in SCS patients (12,13,39).

In this study, we utilized a canonical model of SCS that incorporated anatomical details based on average values in the literature. This canonical model did not account for the inter-patient variability in anatomy and SCS lead placement that has been reflected in interpatient variability in both the amplitude and shape of clinical ECAP recordings (9,22). However, in this study, our goal was to use a canonical model to gain insights into the underlying origin of SCS-induced ECAPs as well as the various physiological and technical factors that affect these recordings. Future studies should consider sources of inter-patient variability and examine their effects on the ECAP recordings.

## CONCLUSION

ECAPs during SCS can be used to investigate neural activation and the corresponding mechanisms of action of clinical SCS. These ECAPs also have the potential to serve as control signals to optimize SCS parameters during closed-loop SCS on a patient-specific basis. However, to successfully interpret these signals, we must understand their origin. In this study, we used a computational model to investigate various technical and physiological factors that affect the composition of these ECAP recordings. Our computational modeling results reproduced several trends observed in clinical data. Our modeling results suggested that clinically effective SCS relies on the activation of numerous axons within a narrow fiber diameter range (i.e., 8.7–10.0  $\mu\text{m}$ ). Model results also suggested that the ECAP amplitude and shape is affected by electrode position relative to the vertebrae as well as the amount of CSF between the recording electrodes and the spinal cord.

## Authorship Statement

Carlos Anaya, Hans Zander, and Dr. Lempka were responsible for the study concept and design. Hans Zander developed the finite element model, and Robert Graham developed the sensory axon models. Carlos Anaya conducted the study, analyzed the data and prepared the manuscript draft, tables, and figures with input and guidance from Dr. Sankarasubramanian and Dr. Lempka. All authors provided intellectual input and assisted with manuscript revisions. All authors approved the final version of the manuscript.

## How to Cite this Article:

Anaya C.J., Zander H.J., Graham R.D., Sankarasubramanian V., Lempka S.F. 2020. Evoked Potentials Recorded From the Spinal Cord During Neurostimulation for Pain: A Computational Modeling Study. *Neuromodulation* 2020; 23: 64–73

## REFERENCES

- Melzack R, Wall PD. Pain mechanisms: A new theory. *Science* 1965;150:971–979.
- Shealy CN, Mortimer JT, Reswick JB. Electrical inhibition of pain by stimulation of the dorsal columns: Preliminary clinical report. *Anesth Analg* 1967;46:489–491.
- Zhang TC, Janik JJ, Grill WM. Mechanisms and models of spinal cord stimulation for the treatment of neuropathic pain. *Brain Res* 2014;1569:19–31. <https://doi.org/10.1016/j.brainres.2014.04.039>.
- Lempka SF, Patil PG. Innovations in spinal cord stimulation for pain. *Curr Opin Biomed Eng* 2018;8:51–60. <https://doi.org/10.1016/j.cobme.2018.10.005>.
- Russo M, Cousins MJ, Brooker C et al. Effective relief of pain and associated symptoms with closed-loop spinal cord stimulation system: Preliminary results of the Avalon study. *Neuromodulation* 2018;21:38–47. <https://doi.org/10.1111/ner.12684>.
- Ertekin C. Studies on the human evoked Electrospinogram: I. The origin of the segmental evoked potentials. *Acta Neurol Scand* 1976a;53:3–20. <https://doi.org/10.1111/j.1600-0404.1976.tb04321.x>.
- Ertekin C. Studies on the human evoked Electrospinogram: II. The conduction velocity along the dorsal funiculus. *Acta Neurol Scand* 1976b;53:21–38. <https://doi.org/10.1111/j.1600-0404.1976.tb04322.x>.
- Maruyama Y, Shimoji K, Shimizu H, Kuribayashi H, Fujioka H. Human spinal cord potentials evoked by different sources of stimulation and conduction velocities along the cord. *J Neurophysiol* 1982;48:1098–1107. <https://doi.org/10.1152/jn.1982.48.5.1098>.
- Parker JL, Karantonis DM, Single PS, Obradovic M, Cousins MJ. Compound action potentials recorded in the human spinal cord during neurostimulation for pain relief. *Pain* 2012;153:593–601. <https://doi.org/10.1016/j.pain.2011.11.023>.
- Parker JL, Karantonis DM, Single PS et al. Electrically evoked compound action potentials recorded from the sheep spinal cord. *Neuromodulation* 2013;16:295–303. <https://doi.org/10.1111/ner.12053>.
- Olin JC, Kidd DH, North RB. Postural changes in spinal cord stimulation perceptual thresholds. *Neuromodulation* 1998;1:171–175.
- Holsheimer J. Which neuronal elements are activated directly by spinal cord stimulation. *Neuromodulation* 2002;5:25–31. <https://doi.org/10.1046/j.1525-1403.2002.2005.x>.
- Lee D, Hershey B, Bradley K, Yearwood T. Predicted effects of pulse width programming in spinal cord stimulation: A mathematical modeling study. *Med Biol Eng Comput* 2011;49:765–774. <https://doi.org/10.1007/s11517-011-0780-9>.
- Laird JH, Parker JL. A model of evoked potentials in spinal cord stimulation. In *Engineering in Medicine and Biology Society (EMBS) 2013 35th Annual International Conference of the IEEE. IEEE*, 2013:6555–6558. <https://doi.org/10.1109/EMBC.2013.6611057>.
- Capogrosso M, Wenger N, Raspopovic S et al. A computational model for epidural electrical stimulation of spinal sensorimotor circuits. *J Neurosci* 2013;33:19326–19340. <https://doi.org/10.1523/JNEUROSCI.1688-13.2013>.
- Howell B, Lad SP, Grill WM. Evaluation of intradural stimulation efficiency and selectivity in a computational model of spinal cord stimulation. *PLoS ONE* 2014;9:e114938. <https://doi.org/10.1371/journal.pone.0114938>.
- Lempka SF, McIntyre CC, Kilgore KL, Machado AG. Computational analysis of kilohertz frequency spinal cord stimulation for chronic pain management. *Anesthesiology* 2015;122:1362–1376. <https://doi.org/10.1097/ALN.0000000000000649>.

18. Parker JL, Laird-Wah J, Cousins MJ. Comparison of a simple model of dorsal column axons with the electrically evoked compound action potential. *Bioelectron Med* 2018;1:117–130. <https://doi.org/10.2217/bem-2017-0006>.
19. Tschirhart CE, Finkelstein JA, Whyne CM. Biomechanics of vertebral level, geometry, and transcorical tumors in the metastatic spine. *J Biomech* 2007;40:46–54. <https://doi.org/10.1016/j.jbiomech.2005.11.014>.
20. Kameyama T, Hashizume Y, Sobue G. Morphologic features of the normal human cadaveric spinal cord. *Spine* 1996;21:1285–1290. <https://doi.org/10.1097/00007632-199606010-00001>.
21. Bozkurt M, Canbay S, Neves GF et al. Microsurgical anatomy of the dorsal thoracic rootlets and dorsal root entry zones. *Acta Neurochir* 2012;154:1235–1239. <https://doi.org/10.1007/s00701-012-1395-0>.
22. Holsheimer J, Den Boer JA, Struijk JJ, Rozeboom AR. MR assessment of the normal position of the spinal cord in the spinal canal. *Am J Neuroradiol* 1994;15:951–959.
23. Grill WM, Mortimer JT. Electrical properties of implant encapsulation tissue. *Ann Biomed Eng* 1994;22:23–33. <https://doi.org/10.1007/BF02368219>.
24. Kilburn KH, Asmundsson T. Anteroposterior chest diameter in emphysema: From maxim to measurement. *Arch Intern Med* 1969;123:379–382. <https://doi.org/10.1001/archinte.1969.00300140025006>.
25. Kao MC, Tsai SK, Tsou MY, Lee HK, Guo WY, Hu JS. Paraplegia after delayed detection of inadvertent spinal cord injury during thoracic epidural catheterization in an anesthetized elderly patient. *Anesth Analg* 2004;99:580–583. <https://doi.org/10.1213/01.ANE.0000130391.62612.3E>.
26. Gaines JL, Finn KE, Slopesma JP, Heyboer LA, Polasek KH. A model of motor and sensory axon activation in the median nerve using surface electrical stimulation. *J Comput Neurosci* 2018;45:29–43. <https://doi.org/10.1007/s10827-018-0689-5>.
27. Graham RD, Bruns TM, Duan B, Lempka SF. Dorsal root ganglion stimulation for chronic pain modulates A $\beta$ -fiber activity but not C-fiber activity: A computational modeling study. *Clin Neurophysiol* 2019;130:941–951.
28. Howells J, Trevillion L, Bostock H, Burke D. The voltage dependence of Ih in human myelinated axons. *J Physiol* 2012;590:1625–1640. <https://doi.org/10.1113/jphysiol.2011.225573>.
29. McIntyre CC, Richardson AG, Grill WM. Modeling the excitability of mammalian nerve fibers: Influence of afterpotentials on the recovery cycle. *J Neurophysiol* 2002;87:995–1006. <https://doi.org/10.1152/jn.00353.2001>.
30. Feirabend HKP, Choufoer H, Ploeger S, Holsheimer J, Van Gool JD. Morphometry of human superficial dorsal and dorsolateral column fibres: Significance to spinal cord stimulation. *Brain* 2002;125:1137–1149. <https://doi.org/10.1093/brain/awf111>.
31. Lloyd SP. Least squares quantization in PCM. *IEEE Trans Inf Theory* 1982;28:129–137. <https://doi.org/10.1109/TIT.1982.1056489>.
32. Hines M, Davison AP, Muller E. NEURON and python. *Front Neuroinform* 2009;3:1. <https://doi.org/10.3389/neuro.11.001.2009>.
33. Towns J, Cockerill T, Dahan M et al. XSEDE: Accelerating scientific discovery. *Comput Sci Eng* 2014;16:62–74. <https://doi.org/10.1109/MCSE.2014.80>.
34. Moffitt MA, McIntyre CC. Model-based analysis of cortical recording with silicon microelectrodes. *Clin Neurophysiol* 2005;116:2240–2250. <https://doi.org/10.1016/j.clinph.2005.05.018>.
35. Lempka SF, Johnson MD, Moffitt MA, Otto KJ, Kipke DR, McIntyre CC. Theoretical analysis of intracortical microelectrode recordings. *J Neural Eng* 2011;8:045006. <https://doi.org/10.1088/1741-2560/8/4/045006>.
36. Lempka SF, McIntyre CC. Theoretical analysis of the local field potential in deep brain stimulation applications. *PLoS ONE* 2013;8:e59839. <https://doi.org/10.1371/journal.pone.0059839>.
37. Bri aire JJ, Frijns JH. Unraveling the electrically evoked compound action potential. *Hear Res* 2005;205:143–156. <https://doi.org/10.1016/j.heares.2005.03.020>.
38. Kent AR, Grill WM. Analysis of deep brain stimulation electrode characteristics for neural recording. *J Neural Eng* 2014;11:046010. <https://doi.org/10.1088/1741-2560/11/4/046010>.
39. He J, Barolat G, Ketic B. Stimulation usage range for chronic pain management. *Analgesia* 1994;1:75–80. <https://doi.org/10.3727/107156994819564401>.
40. He J, Barolat G, Holsheimer J, Struijk JJ. Perception threshold and electrode position for spinal cord stimulation. *Pain* 1994;59:55–63. [https://doi.org/10.1016/0304-3959\(94\)90047-7](https://doi.org/10.1016/0304-3959(94)90047-7).
41. Lempka SF, Zander H, Anaya CJ, Wyant A, Ozinga JG, Machado AG. Model-based analysis of spinal cord stimulation for chronic pain. In: Masia L, Micera S, Akay M, Pons J, editors. *Converging clinical and engineering research on neurorehabilitation III. ICNR 2018. Biosystems & Biorobotics*. Volume 21. Cham: Springer, 2019: 39–43.

## COMMENTS

Recording of evoked compound action potentials (ECAPs) from inactive electrodes during spinal cord system has the potential to allow consistent delivery of stimulation regardless of changes in lead position, but the precise source of these signals is not fully understood. To address this issue, the authors of this study used an established computational model using finite element modeling with

multicompartment models of sensory axons to determine the origin and mechanism by which ECAPs are generated. They found that the model faithfully recreated the triphasic morphology seen experimentally and suggested that the signals are mediated primarily by large axons in the dorsal aspect of the spinal cord of a relatively narrow range of fiber diameters. Changes in ECAPs shape and amplitude were related to electrode location, including position relative to vertebrae, lateral shift, and thickness of CSF layer. They conclude that these results will assist interpretation and implementation of ECAPs for closed-loop spinal cord stimulation.

The results of this experiment validate the use of modeling as a platform for the study of spinal cord stimulation effects, and the fact that the modeled waveforms closely resemble the experimental results is impressive. However, the value of knowledge about precisely how these signals are generated is questionable since it is unclear how this information might advance clinical efficacy. The primary theoretical advantage of the ECAPs closed-loop approach seems to be avoidance of under- or overstimulation via instantaneous normalization of applied current based on its biological effects; in this context, the identity of the source of the feedback signal may not matter as long as it can be recorded. Likewise, the modeled ECAPs signal may be immune to lateral shift, but the fact that different axons are affected based on lead location may have important clinical effects. Nevertheless, the results of this study convincingly demonstrate the power of modeling to discern the effects of neurostimulation.

Jonathan Miller, MD  
Cleveland, OH, USA

\*\*\*

This is an important electrical stimulation modeling study designed to provide new information and insights into the mechanism of ‘closed loop’ spinal cord electrical stimulation. Through rigorous application of cutting edge modeling technologies the authors are able to largely recreate, and predict the compound action potential waveforms that are recorded with the closed loop methodology. The findings provide valuable new insights into the nature of the neural elements within the spinal cord that are activated and then generated the local field potentials that are subsequently recorded.

Matthew Howard III, MD  
Iowa City, IA, USA

\*\*\*

Neuromodulation for pain treatment has not received enough attention in the last years given the important numbers of patients that suffer from chronic pain. Developing new closed-loop methods that utilize some sort of automatic feedback to probe the efficacy of a given stimulation pattern could be critical to increase the improve current therapeutic outcomes of clinical neuromodulation protocols. This paper reports interesting simulations that could offer interpretation to these feedback signals and support the design of modern neuromodulation protocols.

Marco Capogrosso, PhD  
Pittsburgh, PA, USA

Comments not included in the Early View version of this paper.